Dipolar-induced planar anisotropy in ultrathin magnetic films

K. De'Bell
Department of Physics, Trent University, Peterborough, Ontario, Canada K9J 7B8

A. B. MacIsaac, I. N. Booth, and J. P. Whitehead
Department of Physics, Memorial University, St. John's, Newfoundland, Canada A1B 3X7

(Received 7 March 1996; revised manuscript received 26 November 1996)

Monte Carlo simulations are used to study the role of the dipolar interaction in determining the properties of a monolayer of magnetic dipoles on a square lattice. The dipoles are constrained to lie in the plane but are free to rotate within it. Comparison of the Monte Carlo results with those from spin-wave theory indicate that the system orders below a nonzero critical temperature. The effect of the thermally induced anisotropy on the spin-wave spectrum and its role in stabilizing the ordered phase at low temperatures is discussed. Results for the correlation function, both above and below the transition temperature, are compared with the corresponding results for the standard XY model. [S0163-1829(97)05021-2]

I. INTRODUCTION

The dipolar interaction is often small when compared to the exchange interaction in magnetic systems but can play a critical role in determining the magnetic properties of two- and three-dimensional magnetic systems. The long-range character of the interaction can change the critical properties of three-dimensional ferromagnetic systems and can stabilize the ferromagnetic phase in two-dimensional systems.[1,2] The dipolar interaction also plays an important role in determining the domain structures magnetic systems exhibit and can give rise to a rich variety of spatially modulated phases in two-dimensional systems.[3,4] In thin magnetic films, the competition between the magnetic surface anisotropy and the dipolar interaction can lead to the existence of a reorientation transition.[5–7]

In this paper we consider a square lattice of magnetic dipoles constrained to lie in the plane of the lattice but free to rotate within it. We restrict our considerations to pure dipolar systems.

It is well known that the ground state of the planar dipolar system is antiferromagnetic. However, in a study of this ground state, Zimmerman *et al.* realized that the situation is more subtle than one might initially suppose.[8] In the particular case of the honeycomb lattice, it can be shown that the ground state is highly degenerate and defines a continuous manifold of spin configurations. Thus while the dipolar interaction does not exhibit a continuous symmetry with respect to rotation of the spins, the degeneracy of the ground state implies the existence of a gapless excitation at zero temperature. In the standard (ferromagnetic exchange interactions only) XY model the existence of gapless spin-wave excitations destroys long-range order at any finite temperature in the thermodynamic limit.[9] This leads us to question if the existence of a gapless spin wave, implied by the continuously degenerate ground state, will suppress the long-range magnetic order at finite temperature even though the dipolar interaction does not manifest a continuous symmetry and is long range in nature.

More recently Prakash and Henley[10] have considered the related problem of a planar spin system in which the spins interact via a nearest-neighbor interaction. The interaction in this model has the same form as the interaction between nearest-neighbor dipoles, but this model neglects the long-range character of the dipolar interaction. Nevertheless the ground state exhibits a degeneracy similar to that of the analogous dipolar system. Using a linearized spin-wave calculation Prakash and Henley have shown that the spin fluctuations induce an effective potential in the free energy that reflects the symmetry of the underlying lattice for both the honeycomb and the square lattice.[10] They conclude that the system will order magnetically at low temperature and refer to this as thermally induced magnetic order.

While the questions relating to the existence of long-range magnetic order in a two-dimensional dipolar system are of interest from the point of view of magnetic thin films, the process whereby order can be induced through thermal disorder is of itself interesting and may have application outside the realm of magnetic thin films. In this paper we determine how the spin-wave results of Prakash and Henley are modified by the long-range character of the dipolar interaction and determine, by means of thorough Monte Carlo simulations, whether or not the planar dipolar system orders at finite temperature. With regard to this last question, it should be noted that it is not sufficient to demonstrate magnetic ordering at finite temperature in a finite system but, rather, it is necessary to determine the dependence of the order parameter on the system size in order to show that the magnetic order persists in the thermodynamic limit $N \rightarrow \infty$.

In Sec. II we outline a spin-wave calculation for the dipolar system and in Sec. III Monte Carlo results for this system are reported. Section IV describes the nature of the two-point correlation function in this system and in Sec. V we summarize the conclusions that can be drawn from a comparison of the spin-wave results and Monte Carlo results. We also the implications of these results for recent neutron-scattering experiments on $ErBa_2Cu_3O_6$.

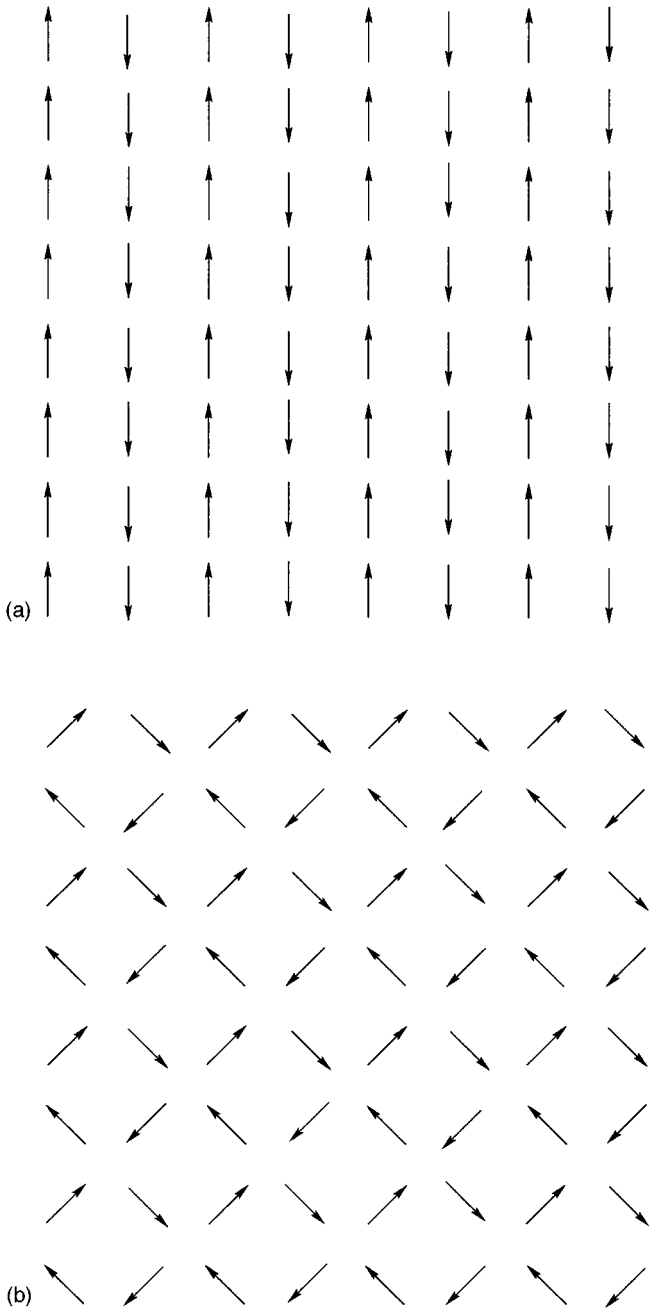

FIG. 1. Two examples of ground-state spin configurations in terms of the original spin variables.

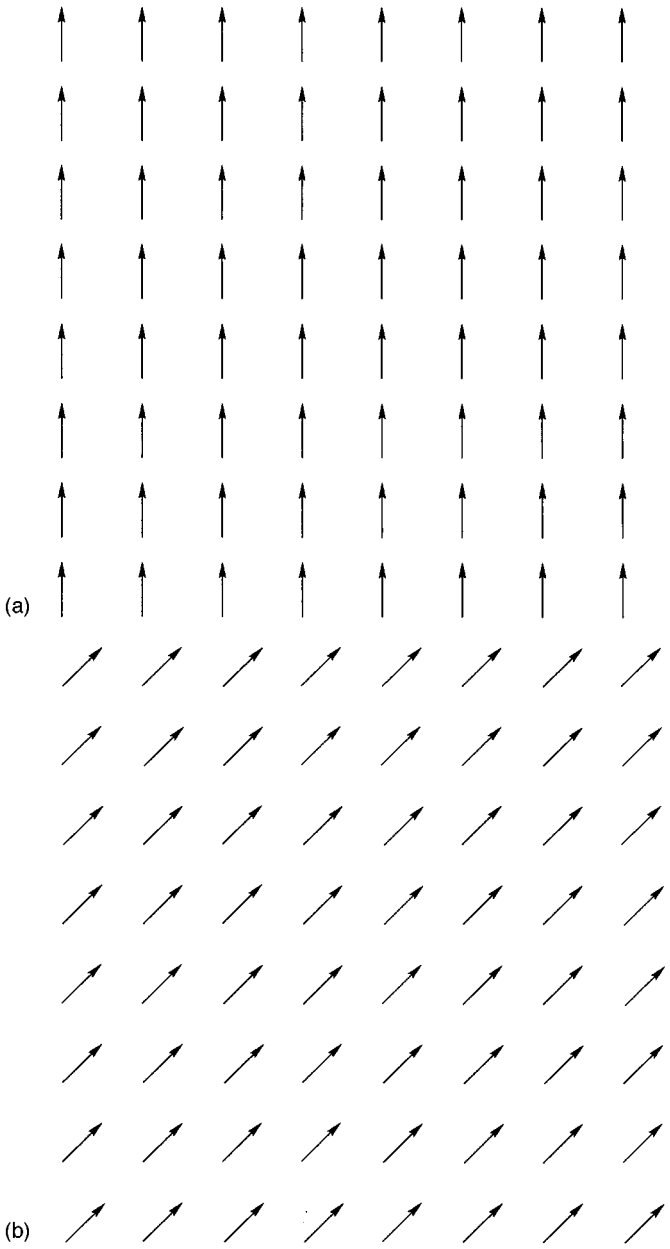

FIG. 2. The ground-state spin configurations corresponding to those in Fig. 1 but shown in the gauge transformed spin variables defined by Eqs. (2) and (3).

II. SPIN-WAVE CALCULATION

The Hamiltonian for the system may be written

$$H=\sum_{ij}\frac{\vec{\sigma}(\vec{r}_i)\cdot\vec{\sigma}(\vec{r}_j)r_{ij}^2-3[\vec{\sigma}(\vec{r}_i)\cdot\vec{r}_{ij}][\sigma(\vec{r}_j)\cdot\vec{r}_{ij}]}{r_{ij}^5}, \quad (1)$$

where the spin vectors $\vec{\sigma}(\vec{r})$ are confined to lie in the XY plane.

The ground-state spin configurations for the dipolar Hamiltonian of Eq. (1) form a continuously degenerate manifold of antiferromagnetic states. Two ground-state spin configurations are shown in Fig. 1. The spin configurations that make up the ground-state manifold are best parametrized by transforming the spins variables $\vec{\sigma}$ by means of a gauge transformation defined by

$$S^x(\vec{r})=(-1)^{n_y/a}\sigma^x(\vec{r}), \quad (2)$$

$$S^y(\vec{r})=(-1)^{n_x/a}\sigma^y(\vec{r}), \quad (3)$$

where a is the lattice spacing, n_x and n_y are the number of steps on the lattice in the x and y directions measured relative to an arbitrary origin, and $\vec{S}$ denotes the transformed spins.

The ground-state configurations, shown in Fig. 1 in terms of the original spin variables $\vec{\sigma}$, are shown in Fig. 2 in terms

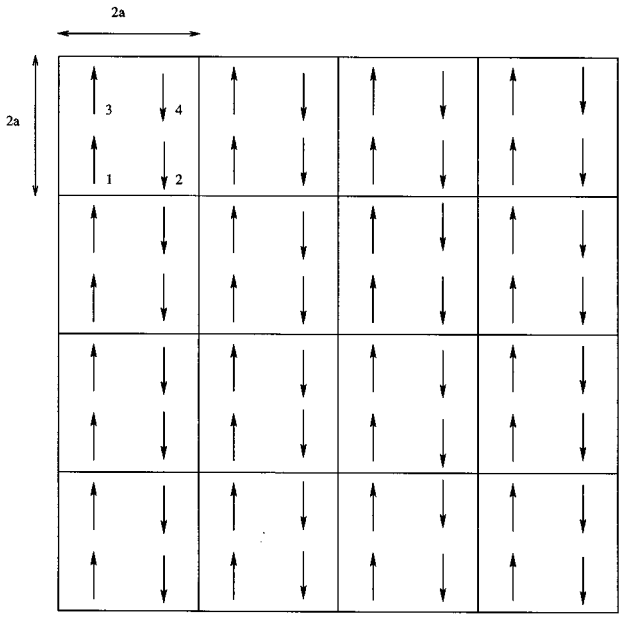

FIG. 3. Magnetic superlattice used in the spin-wave calculation, showing the labeling of the individual spins within the unit cell.

of the gauge-transformed spin variables $\vec{S}$. The obvious merit of the gauge transformation defined by Eq. (3) is that, for the ground-state configurations shown in Fig. 2, the spin variables $\vec{S}(\vec{r})$ are all oriented in the same direction. These ground states may be characterized in terms of the orientation of the two-dimensional order parameter defined by the vector

$$\vec{V}=\frac{1}{N}\sum_{\vec{r}}\vec{S}(\vec{r}), \tag{4}$$

and, more generally, for all ground-state spin states it can be shown that the spin variables $\vec{S}(\vec{r})$ are all parallel so that the ground state may be parametrized by the orientation of the vector $\vec{V}$ defined by Eq. (4). However, it should be noted that the rotational invariance of the energy with respect to rotation of $\vec{V}$ refers only to states belonging to the ground-state manifold and does not imply the existence of global invariance with respect to rotation of the gauge transformed spin variables $\vec{S}$. This distinction between the rotational invariance within a manifold of states and a global invariance of the Hamiltonian under rotation is critical in understanding the behavior of the system.

The low-temperature properties of the spin system may be analyzed by considering small amplitude fluctuations about a ground-state spin configuration. Given the antiferromagnetic character of the ground-state spin configurations, we introduce the lattice shown in Fig. 3 with lattice spacing $2a$ and four spins per unit cell. Labeling the four spins in the unit cell as shown, we express the gauge transformed spin variable in terms of the fluctuation fields as

$$S_x(\vec{r})=\cos\theta_\alpha(\vec{R}_i) \tag{5}$$

$$\approx\cos\theta_0-\sin\theta_0\,\delta\theta_\alpha(\vec{R}_i)-\frac{1}{2}\cos\theta_0\,\delta\theta_\alpha(\vec{R}_i)^2\ldots, \tag{6}$$

$$S_y(\vec{r})=\sin\theta_\alpha(\vec{R}_i) \tag{7}$$

$$\approx\sin\theta_0+\cos\theta_0\,\delta\theta_\alpha(\vec{R}_i)-\frac{1}{2}\sin\theta_0\,\delta\theta_\alpha(\vec{R}_i)^2\ldots, \tag{8}$$

where θ_0 refers to the orientation of the order parameter with respect to the x axis and we have defined the fluctuation in the orientation of the α spin in the unit cell at position $\vec{R}_i$ as

$$\delta\theta_\alpha(\vec{R}_i)=\theta_\alpha(\vec{R}_i)-\theta_0. \tag{9}$$

To leading order in the fluctuations the Hamiltonian may be written as

$$\mathcal{H}=E_0+\sum_{ij}\sum_{\alpha\beta}\delta\theta_\alpha(\vec{R}_i)G_{\alpha\beta}(\vec{R}_i-\vec{R}_j)\,\delta\theta_\beta(\vec{R}_j)+\ldots, \tag{10}$$

$$=E_0+\sum_{\alpha\beta}\int_\Omega d\vec{q}\,\delta\theta_\alpha(\vec{q})G_{\alpha\beta}(\vec{q})\,\delta\theta_\beta(-\vec{q})+\ldots, \tag{11}$$

where Ω denotes the first Brillouin zone. The derivation and the specific form of $G_{\alpha\beta}(\vec{q})$ is given in the Appendix.

The above expression for the Hamiltonian reduces to a single sum by expanding the fluctuation fields in terms of the eigenvectors determined by the equation

$$\sum_\alpha G_{\alpha\beta}(\vec{q})\Phi^\omega_\alpha(\vec{q})=\lambda_\omega(\vec{q})\Phi^\omega_\beta(\vec{q}), \tag{12}$$

where $\omega=0,1,2,3$ and the eigenvalue $\lambda_0(\vec{q})$ is defined so that $\lim_{q\to0}\lambda_0(\vec{q})=0$. The eigenvalue spectrum of this equation depends on the orientation of the order parameter given by θ_0. Two eigenvalue spectrum are shown in Fig. 4 for the case in which the order parameter is oriented along the x axis ($\theta_0=0$). Two features should be noted. First we see that both spectra contain a branch that goes to zero in the limit $q\to0$. This is a consequence of the fact that the ground-state energy defines a continuously degenerate manifold of spin configurations associated with a continuous rotation of the unit vector $\vec{V}$. Secondly we note that in the second branch the eigenvalue spectrum in Fig. 4(b) varies linearly with q in the limit $q\to0$. The corresponding eigenvectors define oscillations in the net magnetization of the lattice. The linear portion of the eigenvalue spectrum arises as a consequence of the nonanalytic nature of the propagator $G_{\alpha\beta}(\vec{q})$ in the limit $q\to0$, reflecting the long-range character of the dipolar interaction. The results for the ''nearest-neighbor'' interaction model used by Prakash and Henley are included for comparison.

The eigenvalue spectrum of the soft mode can be described, in the long-wavelength limit, in terms of a spin-wave stiffness D defined as

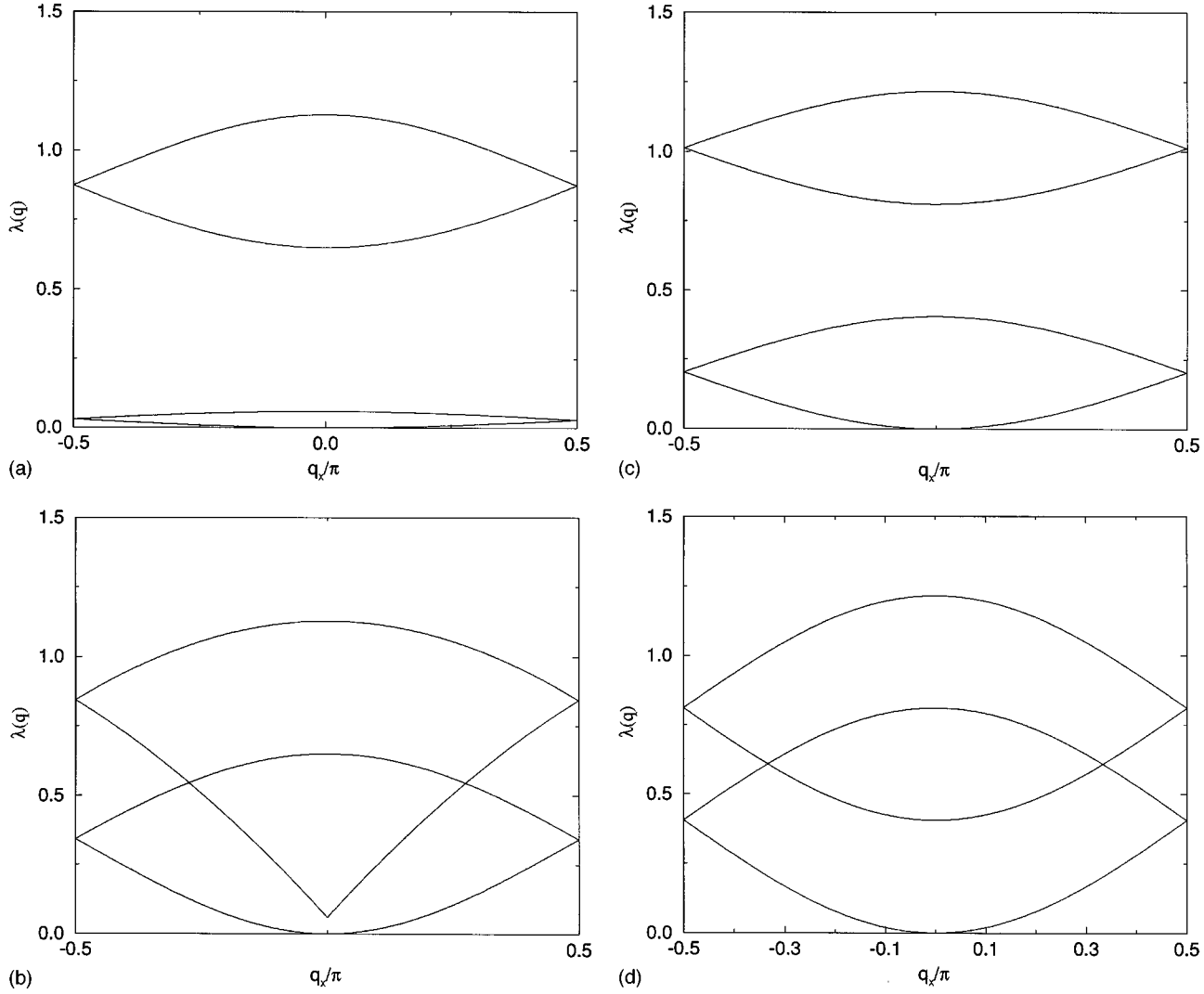

FIG. 4. Eigenvalue spectra for wave vectors directed along the *x* axis (a) and at 45° to the *x* axis (b). The corresponding spectra obtained for the nearest-neighbor interaction used by Prakash and Henley are shown for comparison [(c and d)].

$$\lim_{q\to 0}\lambda_0(\vec{q}) = D(\hat{q})q^2. \tag{13}$$

The spin-wave stiffness is plotted in Fig. 5 as a function of the direction of the wave vector for the case in which the orientation of the order parameter is parallel to the *x* axis and for the case in which the order parameter is orientated at 45° to the *x* axis. Note that it reflects the fourfold symmetry of the underlying lattice. The results for the corresponding ''nearest-neighbor'' interaction used by Prakash and Henley are included for comparison.

The free energy may also be calculated in the linearized spin-wave approximation as

$$F = E_0 + \frac{Nk_BT}{8\pi^2}\int_\Omega d\vec{q}\ln(\det G(\vec{q})) - \frac{Nk_BT}{2}\ln\left(\frac{Nk_BT}{8\pi}\right)$$

$$= E_0 + \frac{Nk_BT}{8\pi^2}\int_\Omega d\vec{q}\sum_\omega \ln\lambda_\omega(\vec{q}) - \frac{Nk_BT}{2}\ln\left(\frac{Nk_BT}{8\pi}\right). \tag{14}$$

While the ground-state energy of the system is invariant under the rotation of the order parameter, the correction arising from the spin-wave fluctuations is not. The resultant change in the free energy is plotted as a function of the orientation of the order parameter in Fig. 6. The orientational dependence of the free energy reflects the fourfold symmetry of the underlying lattice, with a minimum corresponding to the case in which the order parameter is aligned parallel to either the *x* or the *y* axis. The results for the corresponding ''nearest-neighbor'' interaction are included for comparison.

The breaking of the rotational invariance by the thermal fluctuations gives rise to an effective anisotropic field. The amplitude of the field increases with increasing temperature and manifests the fourfold symmetry of the underlying lattice. The appearance of this anisotropic field serves as the basis for order induced by thermal disorder. It should be noted however that while the fourfold anisotropy of the free energy can be obtained from the linearized spin-wave theory described above, to obtain a finite order parameter requires

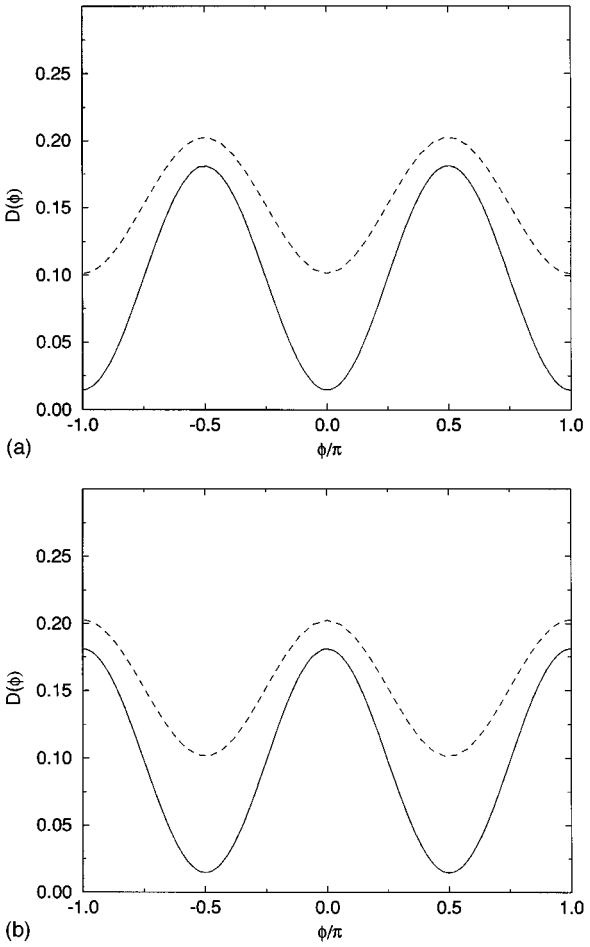

FIG. 5. Spin-wave stiffness (solid line) for order parameters directed along the x axis (a) and at 45° to the x axis (b). The corresponding results for the nearest-neighbor interaction used by Prakash and Henley are also shown (dashed line).

that we include the higher-order terms in the spin-wave expansion of the Hamiltonian given by Eq. (11) in a self-consistent manner.[11]

III. MONTE CARLO

The results of our Monte Carlo simulation show that the system orders at low temperature. Within the new gauge, the order parameter becomes the average magnetization

$$\Psi = \langle |\vec{V}| \rangle = \frac{1}{N} \left\langle \left| \sum_{\vec{R}} \vec{S}(\vec{R}) \right| \right\rangle . \tag{15}$$

In Fig. 7 we plot this as a function of the temperature for systems ranging from $N=64$ to $N=16\,384$. The associated susceptibility, χ, is defined to be

$$\chi = \frac{1}{T^2 N} [\langle |\vec{V}|^2 \rangle - \langle |\vec{V}| \rangle^2]. \tag{16}$$

This is shown in Fig. 8. The peak in the susceptibility coincides with a sharp drop in the order parameter and has features consistent with a continuous transition. One can also see evidence of a phase transition in the heat capacity which is shown in Fig. 9. Assuming that the system has a continuous order-disorder transition, standard finite-size analysis of the size dependence of the transition temperature gives, in the limit of an infinite system, $T_c = 1.39 \pm 0.05$. The error estimate reflects the small system sizes used. An attempt to extract critical exponents has been deferred until larger systems can be studied with more accuracy.

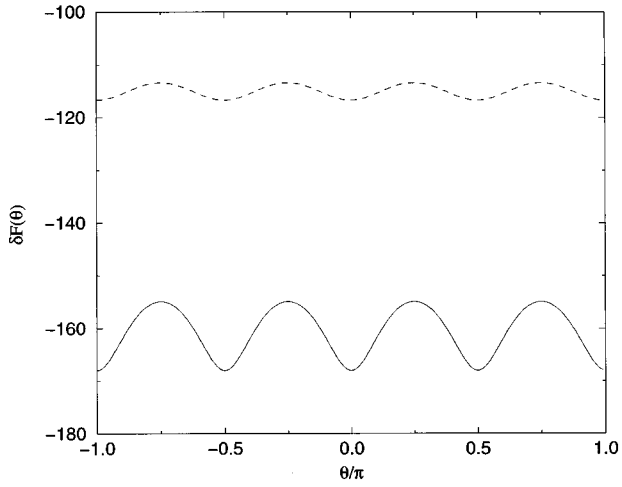

FIG. 6. Variation of the free energy with the orientation of the order parameter (relative to the x axis) in the spin-wave calculation (solid line). Shown is the second term of Eq. (14) in units of $(Nk_BT/8\pi^2)$. The corresponding results for the nearest-neighbor interaction used by Prakash and Henley are also shown (dashed line).

A 16×16 segment of a typical spin configuration, obtained from the Monte Carlo simulations on a 40×40 lattice is shown in Fig. 10 for $(T/T_c=0.7)$. Inspection of this figure reveals a high degree of ordering among the spins. The corresponding spin configuration for the standard XY model is shown in Fig. 11. These are clearly qualitatively different from those shown in Fig. 10 for the dipolar system, in particular the spins are substantially less ordered, due to the presence of the vortices/antivortices.

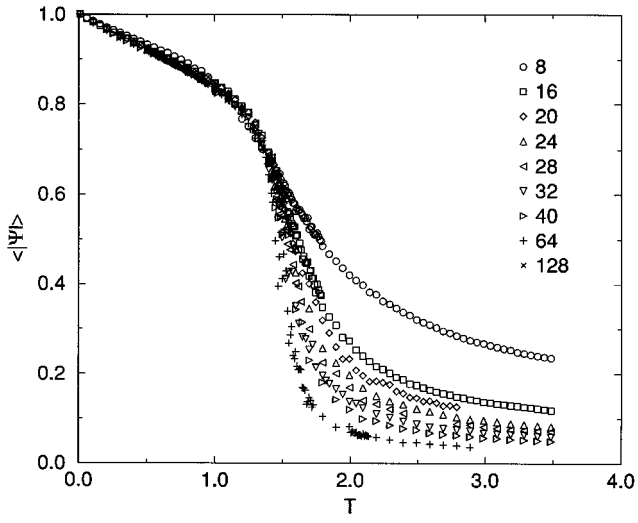

FIG. 7. Monte Carlo results for the order parameter, Ψ, defined by Eq. (16) as a function of temperature. Results are shown for various values of L, the linear size of the system.

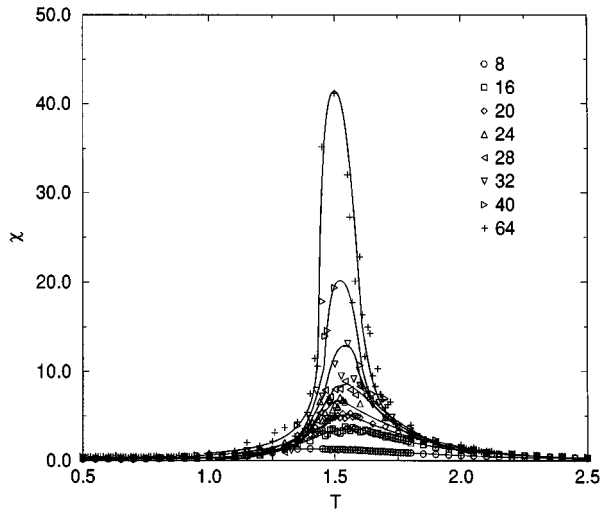

FIG. 8. Monte Carlo results for the susceptibility χ, defined by Eq. (17) shown as a function of temperature.

One must be cautious when interpreting the results of Monte Carlo simulations on finite size systems, in low-dimensional systems. For example, in the case of the standard XY model it is well known that while the magnetization is identically zero at all finite temperatures in the thermodynamic limit,[9] finite-size systems exhibit an ordered phase.[12]

To study the size dependence of the order parameter, we note that Ψ varies almost linearly with temperature at low temperatures (see Fig. 12). This linear behavior arises as a consequence of the thermal excitations of the spin waves. Therefore, we may characterize the temperature dependence of the order parameter at low temperature by the coefficient of the linear term

$$A = \lim_{T\to 0}\left(\frac{1-\Psi}{T}\right). \tag{17}$$

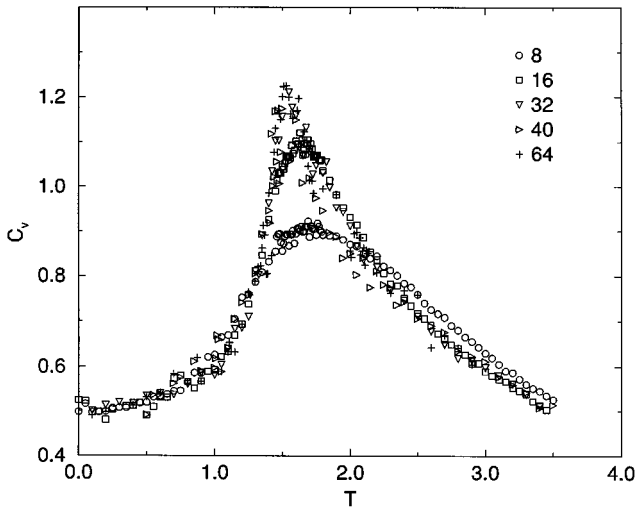

FIG. 9. Monte Carlo results for the magnetic heat capacity as a function of temperature.

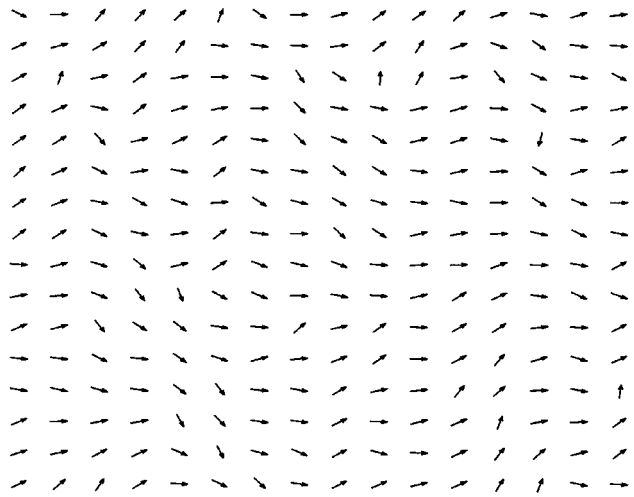

FIG. 10. A 16×16 segment from a typical spin configuration for a 40×40 lattice generated by Monte Carlo simulation of the dipolar planar model at $T/T_c=0.70$.

Calculating A from linearized spin-wave theory yields the result that

$$\lim_{N\to\infty} A(N) \sim \frac{1}{\mathcal{D}}\ln N, \tag{18}$$

where $\mathcal{D}$ is the spin-wave stiffness averaged over the angle.

The divergence of A in the limit $N\to\infty$ is a consequence of the presence of a gapless branch in the linearized spin-wave theory spectrum, which arises from the degeneracy of the ground state. A similar result holds in the case of the standard XY model.[12] The divergence of A would appear to imply the absence of magnetic order at any finite temperature, as is the case in the standard XY model. In Fig. 13 we have plotted the coefficient A obtained from Monte Carlo simulations as a function of $\ln N$. While A has a linear dependence on $\ln N$ at small values of N, the results differ dras-

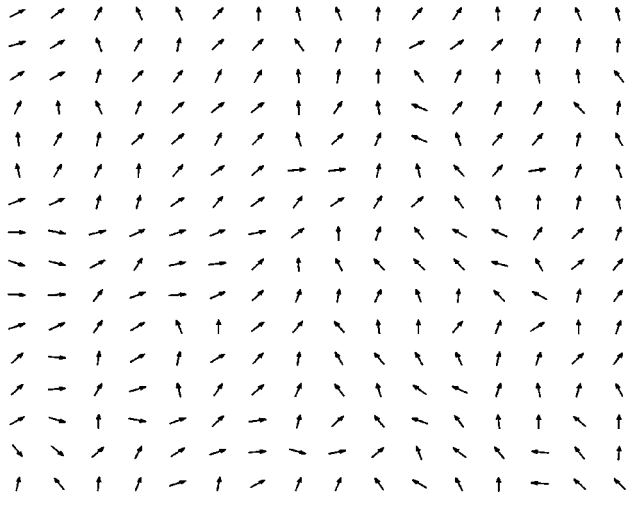

FIG. 11. A 16×16 segment from a typical spin configuration for a 40×40 lattice generated by Monte Carlo simulation of the standard XY model at $T/T_K=0.70$.

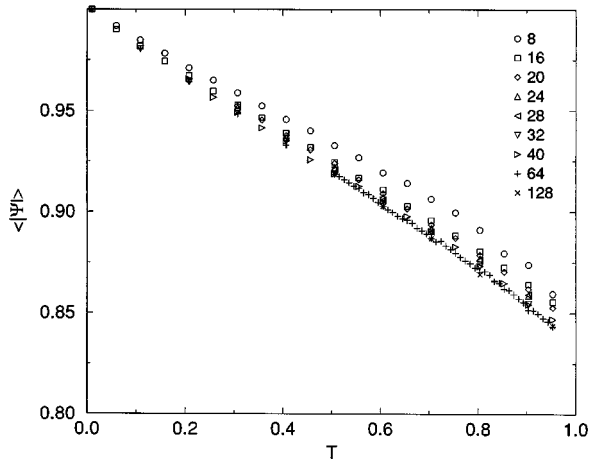

FIG. 12. An expanded plot of the low temperature region in Fig. 7, showing the order parameter Ψ as a function of temperature.

tically from those predicted by linearized spin-wave theory [Eq. 18]. Not only is the slope in the linear region two orders of magnitude smaller than that predicted by the linearized spin-wave theory but, also, the Monte Carlo data appear to approach a plateau as N is increased implying that $A(N)$ has a well defined finite value in the thermodynamic limit given by $\lim_{N\to\infty}A(N)=0.16\pm0.1$. This leads to conclusion that the system will exhibit long-range magnetic order, at finite temperatures, in the thermodynamic limit.

This discrepancy between the analysis of the Monte Carlo simulation data and the linearized spin-wave theory may be understood by noting that the linearized spin-wave theory predicts a gapless mode in the spin-wave excitation spectrum even at finite temperature. However, as shown in the section on spin-wave theory above, the lack of global invariance with respect to rotation of the spin variables $\vec{S}(\vec{r})$ leads to an anisotropy, with respect to rotation of the order parameter, in the free energy at any finite temperature. A self-consistent treatment of the anisotropy requires a renormalized treatment

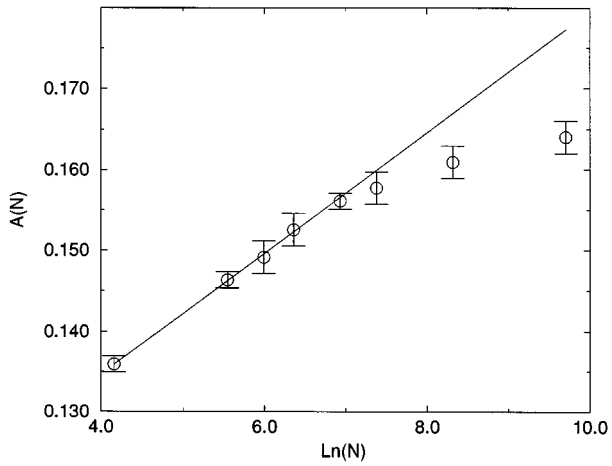

FIG. 13. Monte Carlo results for the coefficient $A(N)$, defined by Eq. (18), as a function of ln$N$. The straight line is a least-squares fit of the lowest four points, which is intended simply as a guide to the eye. The linear dependence predicted by linearized spin-wave theory would have a slope two orders of magnitude larger.

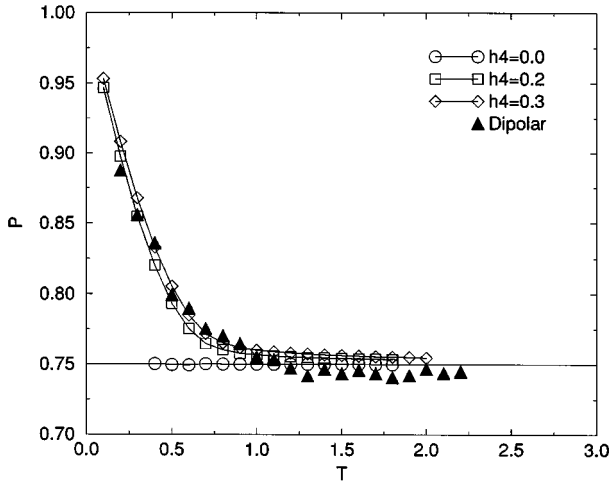

FIG. 14. Monte Carlo results for $P(T)$, the field conjugate to the effective anisotropy and defined by Eq. (20), as a function of temperature. Data for the XY model with exchange interactions and $h_4=0$, $h_4=0.2$, and $h_4=0.3$ are shown for comparison.

of the spin waves to take account of higher-order terms in the expansion.[11] The anisotropy will manifest itself as a gap in the renormalized spin-wave spectra. The presence of a gap in the renormalized spin-wave spectrum implies that the coefficient A, defined by Eq. (17), will yield a well defined finite value in the limit $N\to\infty$. In view of this, we conclude that the observed ordering of the spins $\vec{S}(\vec{r})$ is an effect of a gap in the excitation spectrum and not merely an artifact of the finite system size.

In order to better understand the role of thermally induced anisotropy, we note that its effect locally will be similar to introducing a temperature-dependent anisotropy term $h_4(S_x^4+S_y^4)$ into the Hamiltonian.[10] We define $P(T)$ to be the field conjugate to $h_4(T)$,

$$P(T)=\left\langle \sum_{\vec{R}} (S_x^4+S_y^4) \right\rangle, \tag{19}$$

and measure $P(T)$ for systems of size between $N=576$, and $N=4096$. If the net magnetization is fixed along one of the $\pm y$ or $\pm x$ axis then P is equal to 1, if instead the system is free to orientate itself in any direction then $P=0.75$. Figure 14 shows P as a function of temperature for the pure dipolar system, the standard XY model and the standard XY model with an anisotropy term of the form $h_4(S_x^4+S_y^4)$. For the standard XY model $P=0.75$ at all temperatures, reflecting the orientational freedom of the spins. For the dipolar system the data extrapolates to $P=1$ at $T=0$ indicating that the system orders completely and along one of the lattice axes. As T increases P decays until it is fluctuating about 0.75 well before the transition is reached. Adding the anisotropic field to the standard XY model suppresses the orientational freedom of the spins at low temperature to give a value of P that extrapolates to 1 in the limit $T\to0$. We note that choosing $h_4=0.2$ yields a temperature dependence for P similar to that found for the pure dipolar case.

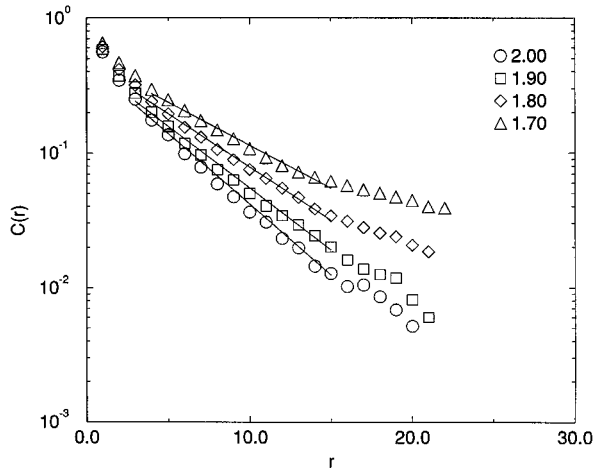

FIG. 15. Dependence of the correlation function, defined by Eq. (21), on distance r for various temperatures above T_c, in a $N=64\times64$ system.

IV. CORRELATION FUNCTION

The results reported above for P indicate that the effective anisotropy in the vicinity of T_c and in a region below T_c is very small when compared with k_BT. It is therefore natural to ask to what extent the system behaves like an isotropic system. To obtain some insight into this we have calculated the two-point correlation function both above and below the transition temperature. The two-spin correlation function is defined in our transformed gauge by

$$C(\vec{r})=\langle\vec{S}(0)\cdot\vec{S}(\vec{r})\rangle-\langle\vec{S}(0)\rangle\langle\vec{S}(\vec{r})\rangle. \tag{20}$$

In the isotropic XY model with exchange interactions only, the transition is the Kosterlitz-Thouless transition.[13] However in the anisotropic XY model with a large anisotropy field which reflects the symmetry of the square lattice the behavior is that of a four-state clock model.[14] In either of these cases, as the temperature approaches the critical temperature from above, the dominant dependence of the correlation function on distance is

$$C(\vec{r})\sim\exp(-r/\xi). \tag{21}$$

Moreover, in both of these cases, the correlation length, ξ, diverges as the critical temperature is approached from above.

We estimate the correlation length at high temperature by assuming that the correlation function decays exponentially as described by Eq. (21). Semilog plots of the correlation function as a function of distance at several values of the temperature above the critical temperature are shown in Fig. 15. The data in these plots follow the expected straight line over a range that extends from approximately 5 lattice spacings to 15 lattice spacings. The observed deviation from a straight line outside of this region is not surprising as the scaling form of Eq. (21) is not expected to hold at distances of only a few lattice spacings and for distances approximately equal to half the system size and larger, the finite nature of the lattice might be expected to give rise to finite-size effects.

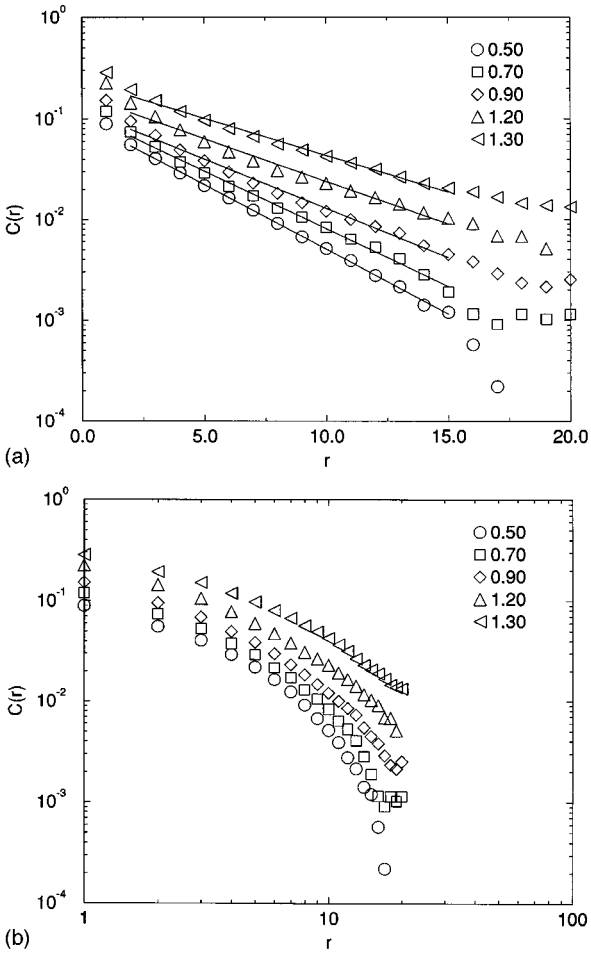

FIG. 16. Dependence of the correlation function, defined by Eq. (21), on distance for various temperatures below T_c, in a $N=64\times64$ system. Data are shown on a semilog (a) and log-log (b) plot.

In principle, it is possible to differentiate between the Kosterlitz-Thouless transition and the conventional ordering transition by determining the dependence of the high-temperature correlation length on temperature as the critical temperature is approached from above.[15] In view of the obvious presence of finite-size effects and the uncertainty in the transition temperature we do not attempt to do so here. Rather, we have analyzed the dependence of the correlation function on distance below T_c in order to provide further evidence for the nature of the transition.

If the transition is an ordering transition such as that observed in the four-state clock model, the correlation function will again have an exponential dependence on distance as described by Eq. (21). However if the system is isotropic, spin-wave theory would predict a power-law dependence on distance

$$C(r)\sim r^{\eta}. \tag{22}$$

For a Kosterlitz-Thouless transition η is temperature dependent and has a value of 0.25 at the transition.

In Fig. 16 the correlation function is plotted as a function of distance at various values of temperature below the critical temperature using both semilog and log-log plots. The

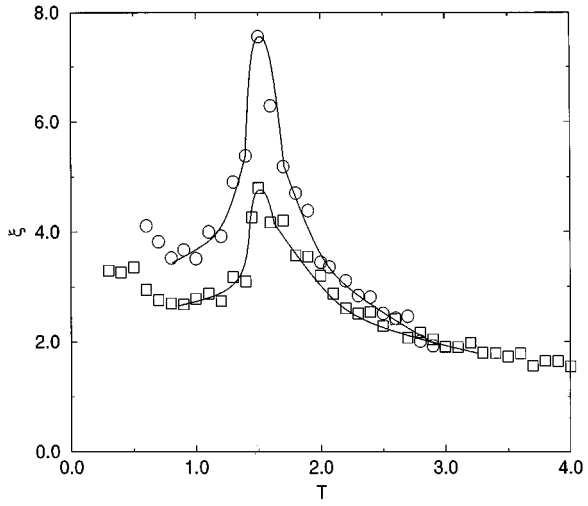

FIG. 17. Correlation length as defined by Eq. (22), calculated from Monte Carlo results and plotted as a function of temperature for both a $N=40\times40$ and a $N=64\times64$ system.

semilog plots are similar to those obtained above T_c (Fig. 15). In particular, a reasonable straight line fit can again be obtained for distances between approximately 5 and 15 lattice spacings. In the case of the log-log plots a straight line can be fitted to only relatively few points at small values of r and the data clearly deviates from this line quite quickly. Thus the dependence of the correlation function on distance at temperatures below T_c seems to have the same exponential form as the dependence above T_c; consistent with the view that the transition is to an ordered state with rotational anisotropy.

The variation of the correlation length with temperature, obtained by fitting the correlation function data to the exponential form of Eq. (21) both above and below T_c, is shown in Fig. 17. The sharp narrow peak in the region around T_c with a rapid decrease to small values on either side of the peak is again consistent with the expected behavior for ordering in a system with rotational anisotropy.

V. CONCLUSION

Our Monte Carlo data for the planar XY model with pure dipolar interactions exhibit thermally induced rotational anisotropy, as characterized by the field P defined by Eq. (19), and indicate that the system orders at a critical temperature of $T_c=1.39\pm0.05$. The behavior of the order parameter, in the gauge transformed system defined by Eq. (3), in the vicinity of T_c is consistent with that of a system undergoing an ordering transition and below T_c the order parameter is found to lie along one of the lattice axes. The exponential dependence of the two-point correlation function on distance both above and below T_c is consistent with an ordering transition in a system with rotational anisotropy.

Experience with the isotropic XY model with exchange interactions demonstrates that the occurrence of a nonzero order parameter in the finite systems used in Monte Carlo simulations must be treated with caution when drawing conclusions about the system in the thermodynamic limit. However our Monte Carlo results clearly indicate that the dependence of the order parameter on system size is significantly less than that predicted by linearized spin-wave theory. For the larger systems studied the decrease in the order parameter with system size is small and the order parameter appears to approach a well defined value for large N. We therefore conclude that the system does indeed exhibit an ordered phase at low temperatures.

Despite the ubiquituous nature of the dipolar interaction a detailed comparison of our results with those for experimental systems, is not straightforward. However, one potential application is the ordering of the rare-earth ions in the high-T_c superconducting copper oxides and related materials. There is considerable experimental and theoretical evidence that the Er ions in $ErBa_2Cu_3O_6$ form a quasi-two-dimensional, square lattice in which the ground state of the Er ions is a continuously degenerate spin doublet.[16] Moreover, calculations indicate that the exchange interaction is relatively weak in this compound.[17] Chattopadhyay *et al.* report neutron-scattering results which suggest that the Er ions do indeed order at sufficiently low temperature.[18] However there are certain difficulties associated with the interpretation of these results.[19] Indeed, more recent neutron-diffraction results indicate that the Er spins exhibit only short-range magnetic order down to 60 mK.[20] The apparent absence of long-range magnetic order in the Er sublattice is surprising in light of the results obtained from the present analysis and serves to emphasize the puzzling nature of these compounds and, in particular, the role played by the dipolar interaction.

In performing the spin-wave calculation we have identified features which occur in the system with a full dipolar interaction but not in the nearest-neighbor model of Prakash and Henley. In particular the linear behavior of the second branch of the spin-wave spectra at small q is associated with the long-range nature of the dipolar interaction.

The role of the thermally induced anisotropy near the ordering transition is an important consideration of the present study. Our Monte Carlo data show that the field P, conjugate to the effective anisotropy field h_4, decreases as the temperature is increased in the ordered phase and for values of $T\geqslant1.2$, P fluctuates about the zero anisotropy value of $P=0.75$. This indicates that the effective strength of the thermally induced anisotropy is very small compared with the thermal energy k_BT in this region which includes the critical temperature. As noted by Prakash and Henley, some sense of the probable role of the anisotropy can be obtained by considering results for the exchange interaction XY model with an anisotropy field h_4. Renormalization-group arguments indicate that an anisotropy field with the fourfold symmetry of the lattice will always be relevant and that the Kosterlitz-Thouless transition will be observed only in the case $h_4=0$.[21,22] For nonzero h_4 the renormalization-group calculation predicts a continuous line of fixed points which meet the Kosterlitz-Thouless line of fixed points at T_{KT} on the $h_4=0$ axis. Thus we expect a transition directly from the disordered state to an ordered state with fourfold symmetry for any finite value of the anisotropy. Our Monte Carlo results are entirely consistent with this. However the renormalization results also imply that any exponents determined will be nonuniversal and depend on the specific value of the effective anisotropy strength.

ACKNOWLEDGMENTS

This work is supported in part by the Natural Sciences and Engineering Research Council of Canada. The authors thank the Pittsburgh Supercomputing Center (PSC) and Digital Equipment Corporation (DEC) for providing access to a DEC Alpha 8400 5/300. A.B.M.I. would like to thank the High Performance Computing Centre (HPCC) and Fujitsu Canada, Inc. for the use of the Fujitsu VPX240 as part of the HPCC scholarship program.

APPENDIX: CALCULATION OF THE SPIN-WAVE PROPAGATOR

The Hamiltonian may be written in terms of the gauge transformed spin variables $\vec{S}_p(\vec{R})$,

$$\mathcal{H}=\sum_{p,q=1}^{4}\sum_{n,m}{}' S_p^{\alpha}(\vec{R}_n)A_{pq}^{\alpha\beta}\Gamma_{pqnm}^{\alpha\beta}S_q^{\beta}(\vec{R}_m), \tag{A1}$$

where $A_{pq}^{\alpha\beta}$ is given by

$$A_{pq}^{\alpha\beta}=(-1)^{\frac{|\mathbf{r}_p-\mathbf{r}_p^{\alpha}|}{a}+\frac{|\mathbf{r}_q-\mathbf{r}_q^{\beta}|}{a}}. \tag{A2}$$

In these expressions the indices p,q refer to the positions within the unit cell and the indices n,m refer to the superlattice vectors in the superlattice described in Fig. 3. α and β refer to the components of the spin vectors.

In order to obtain an explicit form for the propagator that appears in Eq. (11), we write the Hamiltonian as an expansion in the small fluctuations of the directions of the spin variables $\vec{S}$ relative to a chosen reference direction:

$$\mathcal{H}=E_0+\mathcal{H}_2+\text{higher-order terms}. \tag{A3}$$

E_0 is the ground-state energy and

$$\mathcal{H}_2=\frac{1}{2}\sum_{i,j}\sum_{l',k'=1}^{4}\delta\theta_{i,l'}\frac{\partial}{\partial\theta_{i,k}}\frac{\partial}{\partial\theta_{j,l}}\mathcal{H}|_{\theta_0}\delta\theta_{j,l}, \tag{A4}$$

where the first sum is over the superlattice vectors and the second sum is over positions within the unit cell. The angles $\theta_{l,n}$, are defined such that

$$S_l^x(\vec{R}_n)=\cos(\theta_{l,n}), \tag{A5}$$

$$S_l^y(\vec{R}_n)=\sin(\theta_{l,n}). \tag{A6}$$

After taking the two derivatives and evaluating the result at θ_0, we arrive at the result

$$\mathcal{H}_2=\sum_{i,j}\sum_{l',k'=1}^{4}\delta\theta_{i,l'}\Bigg\{-\delta_{l'k'}\delta_{i,j}\sum_{k=1}^{4}\sum_{m}(1-\delta_{j,m}\delta_{k,k'})\times\sum_{\alpha\beta}B^{\alpha\beta}A_{k'k}^{\alpha\beta}\Gamma_{k'kjm}^{\alpha\beta}+(1-\delta_{i,j}\delta_{l',k'})\times\sum_{\alpha\beta}C^{\alpha\beta}A_{k'l'}^{\alpha\beta}\Gamma_{k'l'ji}^{\alpha\beta}\Bigg\}\delta\theta_{j,k'}. \tag{A7}$$

The matrices B and C are defined by

$$B=\begin{pmatrix}\cos^2(\theta_0) & \sin(\theta_0)\\ \sin(\theta_0) & \sin^2(\theta_0)\end{pmatrix},$$

$$C=\begin{pmatrix}\sin^2(\theta_0) & -\sin(\theta_0)\\ -\sin(\theta_0) & \cos^2(\theta_0)\end{pmatrix}.$$

Taking Fourier transforms we obtain

$$\mathcal{H}_2=\sum_{pq}\int_{\Omega_B}d\vec{Q}\,\delta\theta_p(\vec{Q})G_{pq}(\vec{Q})\,\delta\theta_q(-\vec{Q}), \tag{A8}$$

with

$$G_{pq}(\vec{Q})=-\delta_{pq}\frac{1}{\pi^2}\sum_{\alpha\beta}\sum_{k=1}^{4}\sum_{\vec{R}}(1-\delta_{\vec{R}=0}\delta_{qk})A_{qk}^{\alpha\beta}B^{\alpha\beta}\Gamma_{qk}^{\alpha\beta}(\vec{R})+\frac{1}{\pi^2}\sum_{\alpha\beta}\sum_{\vec{R}}(1-\delta_{\vec{R}=0}\delta_{qp})A_{qp}^{\alpha\beta}C^{\alpha\beta}\Gamma_{qp}^{\alpha\beta}(\vec{R})e^{-i\vec{Q}\cdot\vec{R}}, \tag{A9}$$

or equivalently

$$G_{pq}(\vec{Q})=\delta_{pq}\mathcal{A}_p+\gamma_{pq}(\vec{Q}). \tag{A10}$$

To obtain this compact form for G we have defined

$$\mathcal{A}_p\equiv-\frac{1}{\pi^2}\sum_{\alpha\beta}\sum_{k=1}^{4}A_{pk}^{\alpha\beta}B^{\alpha\beta}\Delta_{pk}^{\alpha\beta}(0), \tag{A11}$$

$$\gamma_{pq}(\vec{Q})\equiv\frac{1}{\pi^2}\sum_{\alpha\beta}A_{pq}^{\alpha\beta}C^{\alpha\beta}\Delta_{pq}^{\alpha\beta}(\vec{Q}), \tag{A12}$$

$$\Delta_{pq}^{\alpha\beta}(\vec{Q})=\sum_{\vec{R}}(1-\delta_{\vec{R}=0}\delta_{qp})\Gamma_{qp}^{\alpha\beta}(\vec{R})e^{-i\vec{Q}\cdot\vec{R}}. \tag{A13}$$

To evaluate $\Delta_{pq}^{\alpha\beta}$ a lattice sum must be performed. This can be expressed in a rapidly convergent form using standard lattice sum methods.[23] For $p \neq q$

$$\Delta_{pq}^{\alpha\beta}(\vec{Q}) = \frac{4}{\sqrt{\pi}} \sum_{\vec{R}} \frac{(R^\alpha + r_{pq}^\alpha)(R^\beta + r_{pq}^\beta)}{|\vec{R} + \vec{r}_{pq}|^5} e^{-i\vec{Q}\cdot\vec{R}} \Gamma\left(\frac{5}{2}; \eta^2 |\vec{R} + \vec{r}_{pq}|\right) - \delta_{\alpha\beta} \frac{2}{\sqrt{\pi}} \sum_{\vec{R}} \frac{e^{-i\vec{Q}\cdot\vec{R}}}{|\vec{R} + \vec{r}_{pq}|^3} \Gamma\left(\frac{3}{2}; \eta^2 |\vec{R} + \vec{r}_{pq}|^2\right)$$
$$- \frac{\sqrt{\pi}}{2} \sum_{\vec{R} \neq 0} \frac{(Q^\alpha + \pi \vec{R}^\alpha/2)(Q^\beta + \pi \vec{R}^\beta/2)}{|\vec{Q} + \pi \vec{R}/2|} e^{-i(\vec{Q} + \pi\vec{R}/2)\cdot\vec{r}_{pq}} \Gamma\left(\frac{1}{2}; \frac{|\vec{Q} + \pi\vec{R}/2|^2}{4\eta^2}\right) - \frac{\pi}{2} \frac{Q^\alpha Q^\beta}{|\vec{Q}|} e^{i\vec{Q}\cdot\vec{r}_{pq}} \mathrm{erfc}\left(\frac{|\vec{Q}|}{2\eta}\right). \tag{A14}$$

For $p = q$

$$\Delta_{pp}^{\alpha\beta}(\vec{Q}) = \frac{4}{\sqrt{\pi}} \sum_{\vec{R}} \frac{(R^\alpha R^\beta)}{|\vec{R}|^5} e^{-i\vec{Q}\cdot\vec{R}} \Gamma\left(\frac{5}{2}; \eta^2 |\vec{R}|\right) - \delta_{\alpha\beta} \frac{2}{\sqrt{\pi}} \sum_{\vec{R}} \frac{e^{-i\vec{Q}\cdot\vec{R}}}{|\vec{R}|^3} \Gamma\left(\frac{3}{2}; \eta^2 |\vec{R}|^2\right)$$
$$- \frac{\sqrt{\pi}}{2} \sum_{\vec{R} \neq 0} \frac{(Q^\alpha + \pi \vec{R}^\alpha/2)(Q^\beta + \pi \vec{R}^\beta/2)}{|\vec{Q} + \pi \vec{R}/2|} \Gamma\left(\frac{1}{2}; \frac{|\vec{Q} + \pi\vec{R}/2|^2}{4\eta^2}\right) + \delta_{\alpha\beta} \frac{4\eta^{-3}}{3\sqrt{\pi}} - \frac{\pi}{2} \frac{Q^\alpha Q^\beta}{|\vec{Q}|} \mathrm{erfc}\left(\frac{|\vec{Q}|}{2\eta}\right). \tag{A15}$$

[1] A. Aharony, in *Phase Transitions and Critical Phenomena*, edited by C. Domb and M. S. Green (Academic, New York, 1976), Vol. 6, p. 357.

[2] S. V. Maleev, Zh. Éksp. Teor. Fiz. **70**, 2375 (1976) [Sov. Phys. JETP **43**, 1240 (1976)].

[3] M. Seul and R. Wolfe, Phys. Rev. Lett. **68**, 2460 (1992); M. Seul and D. Andelman, Science **267**, 476 (1995).

[4] J. Arlett, J. P. Whitehead, A. B. MacIsaac, and K. De'Bell, Phys. Rev. B **54**, 3394 (1996), and references therein.

[5] A. Abanov, V. Kalatsky, V. L. Pokrovsky, and W. M. Saslow, Phys. Rev. B **51**, 1023 (1995).

[6] J. Gay and R. Richter, Phys. Rev. Lett. **56**, 2728 (1986); J. A. C. Bland, C. Daboo, G. A. Gehring, B. Kaplan, A. J. R. Ives, R. J. Hicken, and A. D. Johnson, J. Phys. Condens. Matter **7**, 6467 (1995).

[7] A. B. MacIsaac, J. P. Whitehead, K. De'Bell, and P. H. Poole, Phys. Rev. Lett. **77**, 739 (1996).

[8] G. O. Zimmerman, A. K. Ibrahim, and F. Y. Wu, Phys. Rev. B **37**, 2059 (1988).

[9] N. D. Mermin and H. Wagner, Phys. Rev. Lett. **17**, 1133 (1966).

[10] S. Prakash and C. L. Henley, Phys. Rev. B **42**, 6574 (1990).

[11] J. P. Whitehead, Phys. Essays **9**, 609 (1996).

[12] J. Tobochnik and G. V. Chester, Phys. Rev. B **20**, 3761 (1979).

[13] J. M. Kosterlitz and D. J. Thouless, J. Phys. C **6**, 1181 (1973).

[14] F. Y. Wu, Rev. Mod. Phys. **54**, 235 (1982).

[15] C. Bowen, D. L. Hunter, and N. Jan, J. Stat. Phys. **69**, 1097 (1992).

[16] A. Furrer, P. Allenspach, J. Mesot, U. Staub, H. Blank, H. Mutka, C. Vettier, E. Kaldis, J. Karpinski, S. Rusiecki, and A. Mirmelstein, Eur. J. Solid State Inorg. Chem. **28**, 627 (1991).

[17] A. B. MacIsaac, J. P. Whitehead, K. De'Bell, and K. S. Narayanan, Phys. Rev. B **46**, 6387 (1992).

[18] T. Chattopadhyay, P. J. Brown, B. C. Sales, L. A. Boatner, H. A. Mook, and H. Maletta, Phys. Rev. B **40**, 2624 (1989).

[19] T. W. Clinton and J. W. Lynn, Physica C **174**, 487 (1991).

[20] T. W. Clinton, J. W. Lynn, J. Z. Liu, Y. X. Jia, T. J. Goodwin, R. N. Shelton, B. W. Lee, M. Buchgeister, M. B. Maple, and J. L. Peng, Phys. Rev. B **51**, 15 (1995).

[21] J. V. Jose, L. P. Kadanoff, S. Kirkpatrick, and D. R. Nelson, Phys. Rev. B **16**, 1217 (1977).

[22] D. J. Amit, Y. Y. Goldschmidt, and G. Grinstein, J. Phys. A **13**, 585 (1980).

[23] N. M. Fujiki, K. De'Bell, and D. J. W. Geldart, Phys. Rev. B **36**, 8512 (1987).